AIRS
Algorithm Theoretical Basis Document

Level 1b, Part 2: Visible/Near-Infrared Channels

Version 2.1
15 December 1999

Mark Hofstadter, H. H. Aumann, Evan Manning and Steve Gaiser
Jet Propulsion Laboratory
California Institute of Technology

Catherine Gautier and Shiren Yang
Institute for Computational Earth System Science
University of California, Santa Barbara

JPL D-17004

Table of Contents

1. Introduction

1.1 Algorithm Theoretical Basis Documents

The Level 1b Algorithm Theoretical Basis Document (ATBD) describes the theoretical basis of the algorithms used to convert engineering units or data numbers from the Atmospheric Infrared Sounder (AIRS), the Advanced Microwave Sounding Unit (AMSU), and the Humidity Sounder Brazil (HSB) to physical radiances. Engineering units or data numbers are referred to as a level 1a product, while the level 1b product has units of spectral radiance. The description of the algorithms which convert the level 1b measurements to geophysical units is covered in the Level 2 ATBD.

The Level 1b ATBD is divided into three parts:

- AIRS infrared spectrometer

- AIRS visible/near-infrared channels

- AMSU/HSB Microwave channels.

The following document is the ATBD for the level 1b processing related to the AIRS visible/near-infrared channels (referred to as Vis/NIR). This document assumes that the reader is reasonably familiar with the AIRS instrument (Aumann and Miller 1995). Included is a brief description of the relevant parts of the AIRS instrument necessary to explain references to devices, procedures and tables used by the level 1b algorithms. The AIRS Validation Plan and AIRS Calibration Plan, as well as the IR and microwave ATBD documents, contain useful background material. The AIRS homepage (http://www-airs.jpl.nasa.gov) and the EOS homepage (http://eospso.gsfc.nasa.gov) include the latest versions of these documents. Primary changes in Version 2 are the separation of Vis/NIR into its own document, revisions to the instrument description, and revisions to the radiometric and spatial calibration algorithms. (See Appendix C for details.)

1.2 AIRS Overview

The Atmospheric Infrared Sounder, or AIRS, is a high spectral resolution, infrared grating spectrometer to be flown on the EOS Aqua platform. AIRS also carries four visible and near-infrared detectors. The primary function of AIRS is to obtain global temperature and moisture profiles with much greater accuracy than current systems. This will allow for improved weather forecasting, climate monitoring, and improved visibility into the hydrological cycle. AIRS will also monitor select species, such as ozone, and study clouds. To achieve these goals, AIRS works closely with two microwave instruments, the Advanced

Microwave Sounding Unit (AMSU) and the Humidity Sounder for Brazil (HSB). For more information on the infrared or microwave components of AIRS, as well as the historical background to AIRS, see Parts 1 and 3 of the AIRS Level 1b ATBD document.

The primary function of the AIRS Vis/NIR channels is to provide diagnostic support to the infrared retrievals: setting flags that warn of the presence of low-clouds or highly variable surface features within the infrared field-of-view. (The IR field of view at nadir is ~13.5 km, vs. ~2.3 km for Vis/NIR.) The Vis/NIR channels will also aid in integrating AIRS data with data from the imager on the spacecraft, MODIS. There are also several research products that the Vis/NIR channels support, such as determining cloud physical properties and Earth energy balance studies.

1.3 AIRS Visible/Near-Infrared System

This section describes the properties and hardware configuration of the Vis/NIR assembly. Figure 1.1 shows the approximate spectral response of the four Vis/NIR channels. Channel 1 (0.40 to 0.44 μm) is designed to be most sensitive to aerosols. Channels 2 (0.58 to 0.68 μm) and 3 (0.71 to 0.93 μm) approximate the response of AVHRR channels 1 and 2, respectively, and are particularly useful for surface studies. (AVHRR is an imaging instrument currently carried by NOAA polar orbiting satellites.) Channel 4 has a broadband response (0.48 to 0.95 μm) for energy balance studies.
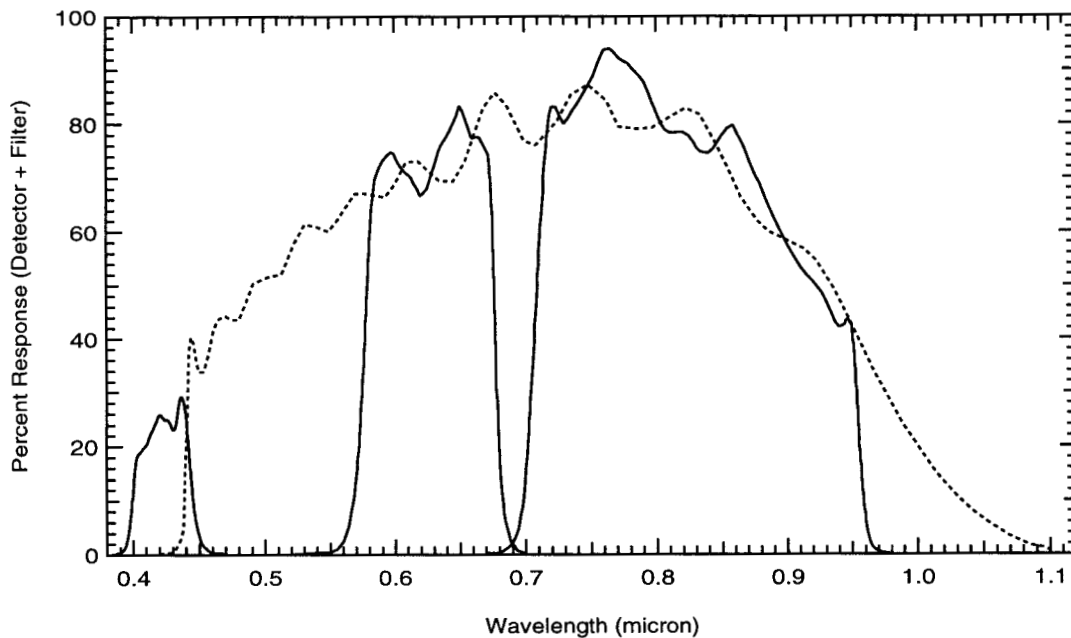

Figure 1.1: Approximate spectral response of the four Vis/NIR channels. The three solid curves are, from left to right, Channels 1, 2, and 3. The dashed curve is the response of Channel 4. Radiation damage over the five-year instrument lifetime will slowly degrade the longwave response of Channels 2, 3, and 4 (see Fig. 1.2).

The spectral response curve of the visible channels is defined by the product of the spectral response of these elements:

 a) The reflectivity of three mirrors (the scan mirror and two fold mirrors).

 b) The transmission characteristics of the field imaging lenses.

 c) Sharp cut-on and cut-off interference filters (except for the long-wave side of channel 4, which uses a pass-filter).

 d) The spectral response curve of the Silicon detectors.

Measurements have been made of the spectral response of all the above items (Hofstadter 1999a and Fig. 1.1), except the lens transmission coefficients. The lenses are not expected to have an appreciable spectral effect, however, and can be ignored in this regard. The scan mirror and the folding mirrors of the optics are Silver coated with a thin layer of SiO_x, using Denton proprietary process FSS99. This coating should have a minimal (< 2%) polarization dependence in the 0.4 to 1.0 μm region, which was too small to detect by the test set-up used during ground characterization of the scan mirror.

The long wavelength spectral extent of Channel 4 is controlled by the cutoff wavelength of the Si diode, which is radiation dose dependent. Figure 1.2 shows the relative response of the Si diode before radiation exposure (pre-rad) and after five years in orbit (post-rad). The spectral response of Channel 4 (and, to a lesser extent, Channels 2 and 3) therefore changes slowly and proportionally to the total radiation dose received. There is no in-orbit capability to directly verify the spectral passband. An empirical spot check validation of the spectral response curves using various ground test sites and algorithms in support of this validation are discussed in Section 3.
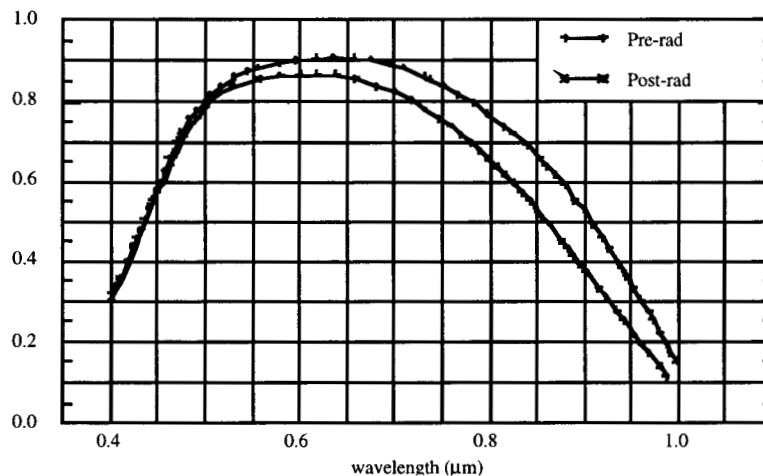
Figure 1.2: The effect of radiation on the spectral response curve of the Si diode. The upper curve (marked "Pre-rad") shows the expected response at launch. The lower curve ("Post-rad") is the expected response after five years in orbit. These data were provided by LMIRIS.

Figure 1.3 is a schematic of the optical layout. Each Vis/NIR channel consists of a linear detector array with nine pixels in the along-track direction. Each pixel has an instantaneous field-of-view (IFOV) 0.190 degrees across-track and 0.149 degrees along-track, with a 0.037 degree gap between adjacent pixels along-track. (Pixel to pixel variations in IFOV have been measured to be less than 0.001 degrees, except for Channel 4, in which at least one pixel has an across-track FWHM of 0.184 degrees.) The diffraction limit of the optics for the four channels is 0.002, 0.006, 0.010, and 0.014 degrees, respectively. Projecting the IFOV on the nadir point from the nominal 705 km orbit, pixels are 2.28 km wide. For comparison, the AIRS infrared footprint is circular and approximately 13.54 km in diameter. Cross-track scanning of the detectors is achieved using the same mirror as is used by the infrared detectors. The four detector arrays are aligned to within 10% of the pixel width. Verification and monitoring of the spatial alignment of the visible detector footprints relative to each other and relative to the infrared footprint is carried out in orbit. Procedures and algorithms for the mapping of the visible channels relative to each other and relative to the infrared footprint is discussed in Section 4.
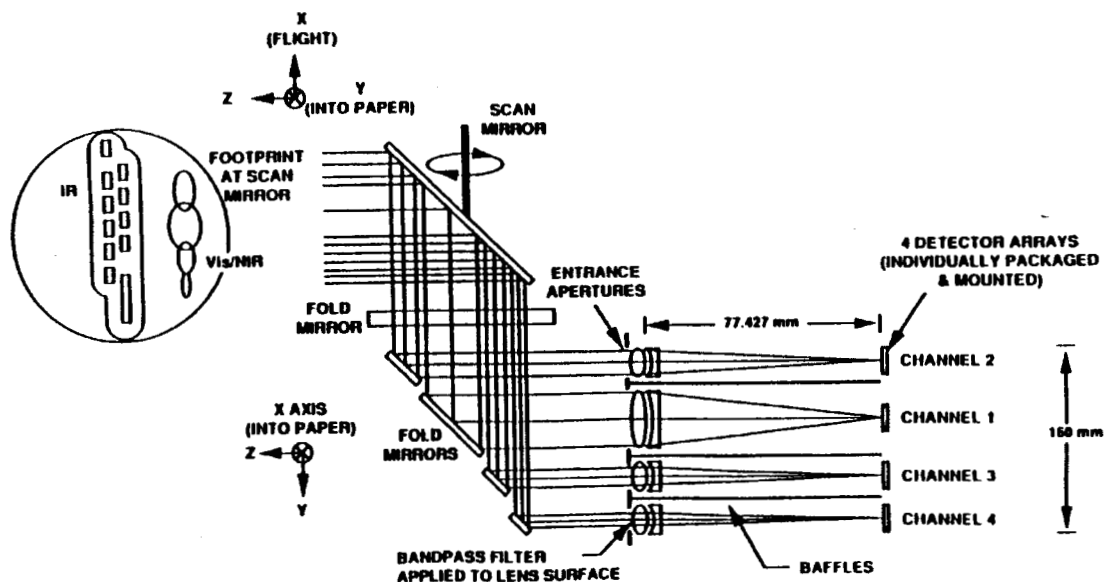
Figure 1.3: Schematic of the optical layout of the Vis/NIR channels. The spectral filters (not shown) are deposited on the detector arrays. Unlike the field of view of all infrared channels, which is defined by a single field stop (see Part 1 of the Level 1b ATBD), the fields of view of the visible channels are defined by the locations of the four arrays in the image planes of the entrance apertures.
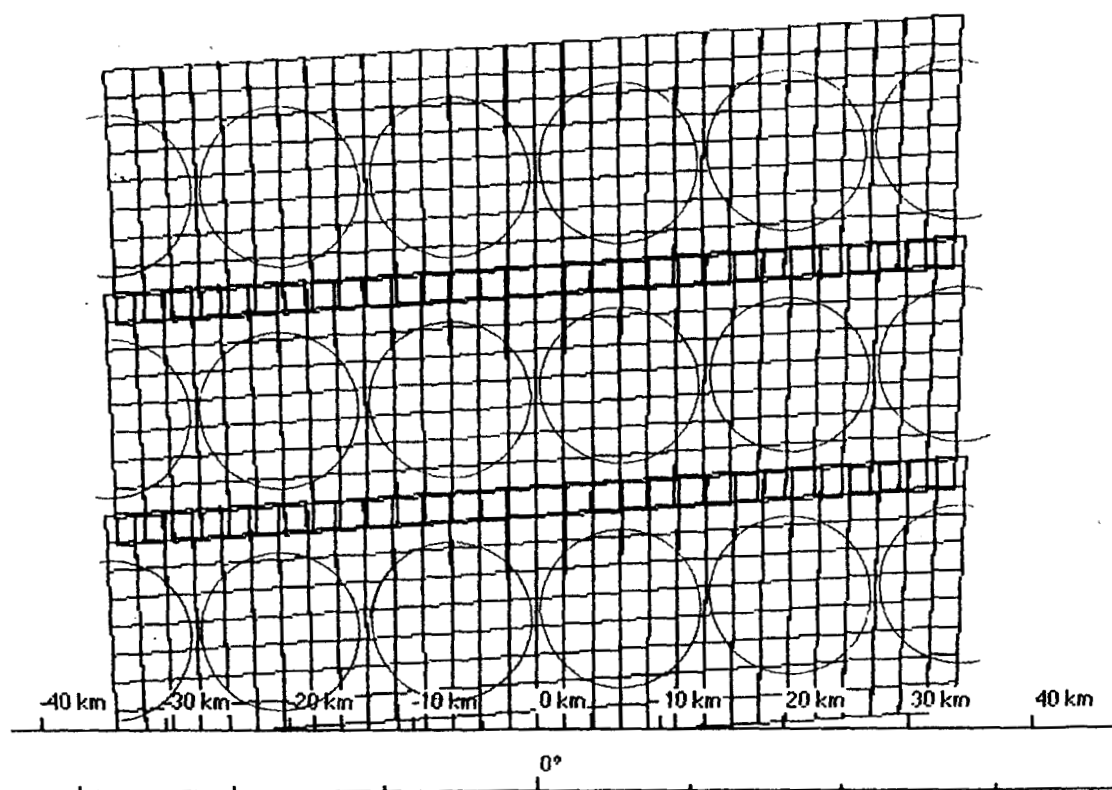
Figure 1.4: Schematic of the ground location of the visible footprints (squares) relative to the circular infrared footprints. The along-track direction is towards the top of the page. Three scan lines are shown near-nadir, for the nominal 705 km orbital altitude. The footprints are only schematic because the surface is oversampled by the Vis/NIR detectors: there are really 8 across-track samples per infrared footprint, resulting in each square pixel overlapping by 1/3 with its neighbors to either side. Similarly, each scan line overlaps with the previous by ~1.57 pixels, but for clarity the figure shows the overlap as only 1 pixel.

Figure 1.4 shows schematically the ground location of the visible footprints relative to the spectrometer footprints near nadir for three scan lines. In the figure, the spacecraft flight direction is towards the top of the page, and the three roughly horizontal rows of circles represent three across-track scans of the instrument. (Spacecraft motion shifts successive samples in the along-track direction.) Each Vis/NIR detector consists of 9 pixels aligned in the along-track direction, which are swept across track by the scan mirror. There are approximately 1.57 pixels of overlap between successive scan lines and eight overlapping pixels across each infrared footprint. (For simplicity, the scan line overlap is shown as one pixel, and only six non-overlapping pixels are shown across track for each infrared footprint.)

Throughout this document, the term "pixel" is used to describe a roughly square region on a detector, 250 μm on a side. Each pixel, however, is composed of 8 sub-elements, a sub-element being 250 μm in the scan direction, $\hat{y}$, but only 25 μm along the array axis, $\hat{x}$. The

eight sub-elements are read individually, but the outputs are added together before being reported by the instrument. The detailed detector layout is shown in Fig. 1.5. To obtain a complete 9 pixel read out, 90 sub-elements are sampled, with only 72 being used to form pixels. (Two sub-elements per pixel are left unused to simplify the readout electronics.) To allow for fine along-track alignment of the channels, each linear array actually contains 128 sub-elements, and the starting point for which 90 sub-elements to sample was adjusted. A final detail to be aware of is that the 90 sub-elements of each channel are read sequentially, with 6 μs between samples. Due to scan mirror motion, this offsets each sub-element 0.157% of a pixel in the across-track direction from the previous sub-element. The offset between the first-used and last-used sub-element of a 9 pixel sample is thus 13.66% of a pixel.
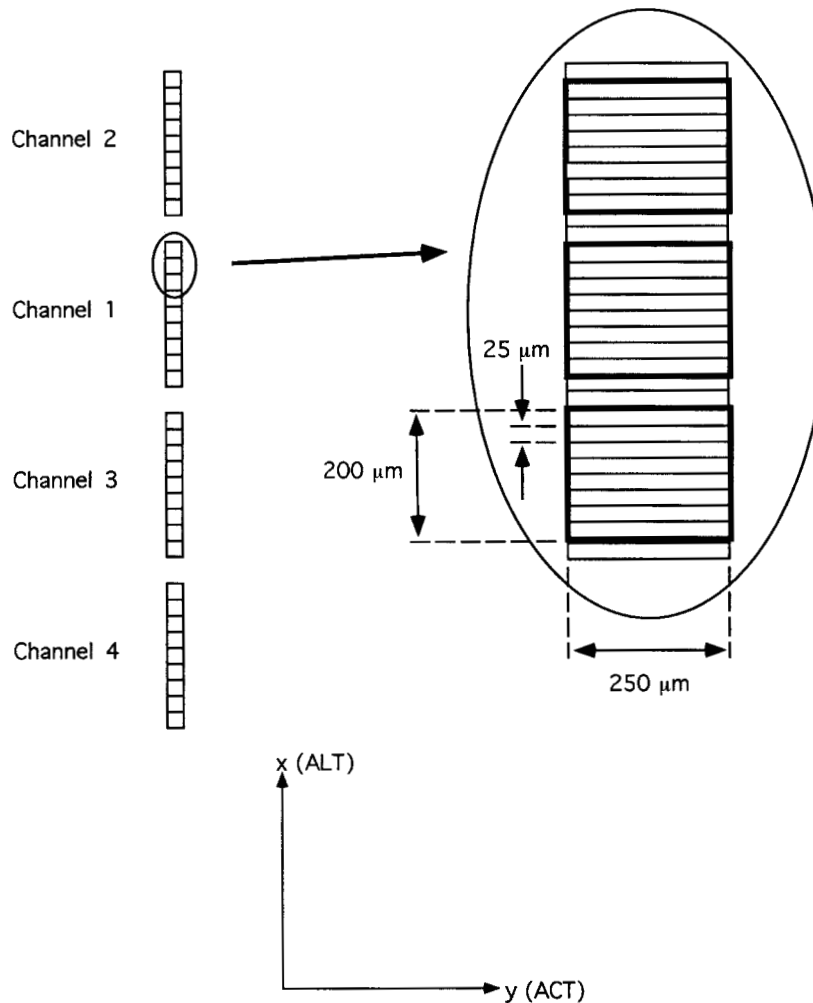
Figure 1.5: Schematic diagram of the layout of visible detectors within the AIRS instrument. Each pixel is 250 μm wide, and is composed of 8 sub-elements. Each sub-element is 25 x 250 μm. Each detector array is aligned to within 0.001 radians of the instrument x-axis (the instrument scans along the y-axis). Note that the x and y axes correspond to the spacecraft's along-track (ALT) and across-track (ACT) directions, respectively. There are two sub-elements between each pixel which are not used in forming the pixels (see text).

As discussed in Section 1.2, the primary purpose of the visible channels is to provide diagnostic support for the IR/microwave temperature and vapor retrievals. For this purpose the spatial alignment between the AIRS visible and infrared footprints must be known to approximately half a pixel diameter, equivalent to ~0.09° or about 1.1 km at nadir. The diagnostic tasks also require stable relative (photometric) response, since the quality indicators are empirically determined. This requirement is consistent with the hardware, which supports stable photometric response, but note that the pre-launch absolute calibration accuracy is good to only 20%.

The secondary purpose of the visible channels is to support research products related to the AIRS core data products. Such research products include downwelling short-wave radiation and determination of the height of low clouds. For these purposes, good relative photometric accuracy and absolute radiometric accuracy to about 5%-10% is needed. This requirement is not supported by the hardware implementation, but can be reached through vicarious calibration and cross-calibration with other instruments, in particular MODIS. This is discussed in Sections 2.3 and 2.4. Simultaneous analysis of MODIS and AIRS data under normal scene contrast conditions would require knowledge of the pixel centroids to about half the diameter of the MODIS pixels, or 0.01-0.04°. This requirement can be considerably relaxed under the low scene contrast conditions typically selected for cross-calibration.

2. Radiometric Calibration

2.1 Introduction

During the launch and operation phases of the EOS spacecraft the performance of the AIRS Vis/NIR channels is expected to change. This may be caused by normal temperature variations in orbit, by a change of the sensor optical alignment during launch, or by changes in sensitivity due to surface contamination and radiation damage over the life of the mission. The sensor is designed to achieve better than 1% *relative* photometric accuracy (channel-to-channel and temporal) at an albedo of unity. There is no absolute calibration accuracy requirement for the Vis/NIR sensors. Though on-board photometric calibration capabilities exist (described below), the calibration accuracy may decrease over time due to lamp degradation and changes within the optical system. Therefore, indirect calibration (vicarious calibration) with known ground surfaces and cross-calibration with other related instruments is planned.

The radiometric calibration algorithm in the Vis/NIR will correct for systematic effects caused by optical system degradation during launch and operation, change of offset and sensitivity of the detectors and electronics, change of spectral response of the detectors with total radiation dose, and non-linearity of the analog-to-digital (A/D) converters. Pre-launch calibration provides the functional relationship between digital counts and radiance, which is the linearized calibration equation:

$$R = \alpha * DN + \beta, \qquad\qquad \text{Eq. 2-1}$$

which can be rewritten as

$$R = \alpha * (DN - DN_o), \qquad\qquad \text{Eq. 2-2}$$

where DN is the (linearized) digital output of the electronics in response to a radiance R received by a Vis/NIR channel, α and β are the gain and offset of the channel, respectively, and DN_o is the digital number corresponding to the dark view. Because a similar calibration algorithm applies to all four Vis/NIR channels, the channel number is not included in the calibration expressions.

Different data products have different calibration accuracy requirements. The accuracy of the radiance measurement can be refined in three steps, with increasing absolute accuracy and algorithmic and operational complexity.

Step I: Makes use of the onboard calibration system to determine the offset and gain.

Step II: Makes use of the onboard calibration system and uses ground based sites (vicarious calibration) to determine a gain correction term.

Step III: Makes use of the onboard calibration system, then uses data from other instruments on the same spacecraft to deduce a gain correction term, γ, so that Eq. 2-2 becomes:

$$R = \gamma \alpha (DN - DN_o). \qquad\qquad \text{Eq. 2-3}$$

The routine calibration algorithm is based entirely on Step I, with the multiplicative gain correction term set equal to unity. Step II will be done off-line at a team member facility on a monthly basis, resulting in the delivery of a table of multiplicative correction coefficients to the onboard calibration. Step III is a research product to be developed at a team member facility. Although the concept of this algorithm will be discussed, details of the algorithm are outside of the scope of this ATBD.

2.2 On-Board Calibration

For Step I the on-board photometric calibration equipment, consisting of a dark target and calibration sources, will be used to calibrate changes in offset and gain. The calibration hardware is described in detail in the AIRS Calibration Plan, available from the web sites referred to in Section 1.1. Summaries are provided here.

2.2.1 Dark View.

The visible detectors view the infrared blackbody once every 2.667 seconds, which serves as the Vis/NIR dark view. This provides the zero signal reference level, or "dark current" for the calibration. (The blackbody is described in the AIRS Calibration Plan.) The albedo of the blackbody in the visible is expected to be less than 0.01. Note that the detector dark current is a strong function of temperature, and that a temperature sensor is used to monitor the detectors.

2.2.2 Visible Light Calibration Source

The visible light calibration source contains three Welch Allyn No. 01178 halogen-filled tungsten lamps rated at 5.0 Volts, 0.44 amp. The lamps are used one at a time: multiple lamps are carried for redundancy and to track changes in bulb output due to use (see below). The bulbs are viewed through a diffuser plate which was intended to minimize geometric effects. The diffuser has proven to be ineffective, however, and calibration lamp brightness varies from pixel-to-pixel within a channel, and from sample-to-sample for a given pixel. In addition, one of the bulbs is found to saturate some pixels, limiting its usefulness as a calibration source. The color temperature of the bulbs is nominally 2925 K. Just prior to submission of this document, however, the instrument manufacturer indicated that the lamps may have been too strongly heat-sinked, preventing the lamps from entering halogen mode. What effect this has is not yet known, but operating at a lower temperature is likely to decrease the color temperature but increase the lifetime from nominal values. The bulb output is passed through a spectral filter to increase the blue/red color-ratio, which approximates the shape of the solar spectrum. The filaments are operated at 4.4 Volts, 0.42 amp (1.9 Watts) to extend the lifetime. At these settings, the continuous operation lifetime of the bulbs is nominally 3300 hours (Hofstadter 1998), but the cooler operating temperatures mentioned above can significantly increase the lifetime. The calibration SNR is dependent on which lamp is being observed. Averaging over the 8 samples each pixel gets of the diffuser plate in a single scanline, the SNR in ground test data for Lamp 1 is ~35, 900, 3300, and 2100, in the four visible channels, respectively. Lamp 2 has similar levels for channels 1 and 2, but saturates in channels 3 and 4. Lamp 3 has SNR levels roughly one-half to one-third those of Lamp 1. One of the three tungsten lamps is operated for about eight minutes once every second orbit. This results in 1771 hours of operation in 5 years, roughly half the nominal continuous operation lifetime of a single bulb. Since the filament output might require about 1 minute to stabilize if halogen-mode were entered, measurements from ~150 looks can be averaged to improve the effective SNR. In practice, however, the lamps do not appear to enter halogen mode, allowing all 180 looks in the 8-minute calibration period to be used.

The output and color temperature of a lamp changes as the filament ages. To monitor this, the following strategy will be employed. (A more mathematical description is given in Section 2.5.4.1.) Calibrations are done approximately every other orbit using bulb A (an arbitrary

designation) of the photocalibration system. Every 200 orbits, a calibration with bulb B will follow bulb A, and every 500 orbits an observation of bulb C will be added. Because bulb C is used so sparingly, it will not degrade significantly and it serves as a standard for age adjustments to the observations of the other bulbs. Bulb B, used a moderate amount, serves as a short-term standard for bulb A and as a consistency check for comparisons of bulbs A and C. Note that if one bulb fails during launch, it is expected that the extra calibration every 500 orbits can be deleted with negligible effect on the calibration accuracy. If two or more bulbs fail on launch, however, vicarious and cross calibration (Sections 2.3 and 2.4) will be necessary to maintain photometric accuracy over the instrument lifetime. As discussed above, Lamp 2 saturates some pixels in channels 3 and 4, making it the logical choice for use as the backup bulb (Bulb C in the above scheme).

Even with the on-board lamps operating, the absolute calibration of the system can be significantly improved through routine vicarious calibration using well characterized ground sites. This process, error estimates, and vicarious calibration update frequencies and relevant algorithms are described in Section 2.3.

2.2.3 Calibration of the gain

The visible detectors view the infrared blackbody every 2.667 seconds. The zero signal reference level of the dark view will be used to determine the offset, DN_o.

The tungsten lamps are used to determine the gain, α, on-board. We have:

$$\alpha(ob) = \frac{R_c}{DN_c - DN_o},$$

Eq. 2-4

where DN_o is the signal (counts) observed from the dark view, DN_c is the signal (counts) observed from the calibration lamp, and R_c is the radiance of the on-board calibration lamp. The label "ob" is used to denote on-board calibration.

2.2.4 Photometric Accuracy Estimate

The Vis/NIR sensor is required to achieve 1% relative photometric accuracy at an albedo of unity. Estimates made at the preliminary design review indicate that the design will achieve this requirement over the full five year mission lifetime. Ground testing was insufficient to confirm this, as the test source used was itself considered unstable at this level. The leading components to the photometric error budget are the stability of the electronics subsystem and the stability of the photometric calibrator.

Response non-linearity in the detectors and electronics is expected to be small. While measurements were made during ground testing, the test setup and equipment was suspect

(Hofstadter 1999b), preventing confirmation of this. Linearity changes occurring during the mission as a result of natural radiation exposure are expected to be less than 0.5%. The gain/offset stability is estimated to be 0.3%. The photometric calibrator contribution to the uncertainty is due to inter-lamp geometry differences, a possible dependence of the calibration signal on ambient temperature, and unknown differences in the aging properties of the bulbs. Insufficient data was collected during ground tests to quantify these factors, but extensive observations during the on-orbit checkout phase (identical to vicarious calibration described in the next section) and the bulb rotation scheme described in Section 2.2.2 will determine the significance of these effects.

Signal-to-noise is not a significant contributor to photometric error. The predicted signal-to-noise ratio at an Earth albedo of 0.4 is greater than 550 for all channels at the start of the mission, degrading to about 420 at the end of the five year mission, at a nominal sensor temperature of 30 C.

2.3 Vicarious Calibration

An improvement in the calibration accuracy is achieved in Step II. There are many vicarious calibration techniques which all have strengths and weaknesses. They include ground-based, aircraft based, satellite-based, buoy based and lunar observations (Abel 1991; Brest and Rossow 1992; Che *et al.* 1991; Che and Price 1992; Fraser and Kaufman 1985; Holben *et al.* 1990; Price 1987; Slater *et al.* 1987). Note that "ground-based" is used here to mean based upon observations of the ground from orbit. The goal of these techniques is to estimate the radiance at the instrument aperture given an observation from one or more instruments and/or a calculation from a radiative transfer model. These techniques are used to obtain the gain of the instrument but cannot provide, in general, the offset. Vicarious calibration helps us to distinguish changes in instrument response from changes in the on-board calibration lamps, and can significantly improve the absolute calibration of the AIRS Vis/NIR system relative to the 20% pre-launch accuracy.

2.3.1 Theoretical Basis

A ground-based vicarious calibration must be done with known, homogeneous ground surface targets with relatively high surface reflectance. The area should be large enough to ensure complete coverage by one sensor pixel. Clear sky over a sand surface, such as White Sands in New Mexico, or other desert areas are good targets (Frouin and Gautier 1987; Slater *et al.* 1991 and Guenther *et al.* 1990). We also intend to make regular use of MODIS ground calibration sites, such as Railroad Valley Playa in Nevada. In order to produce reliable ground-based calibrations, an accurate estimation of the surface reflectivity, the aerosol type and concentration, and the atmospheric profile, particularly the water vapor column density, is essential. (Spectral reflectivity of a sand surface is related to its moisture

content. The difference between dry and wet sand reflectivities in the Visible and NIR wavelengths can be as much as 15% [Walraven and Coulson 1972].) If the solar and viewing zenith angles and relative azimuth angle of the ground objects are large, the BRDF effects must be taken into account. Thus, an accurate measurement (or model) of the target's spectral bi-directional reflectivity is necessary. It has been estimated that the absolute radiometric calibration accuracy that can be obtained using this ground-based approach is better than 13% (Frouin and Gautier 1987).

2.3.2 Sensitivity Analysis

To evaluate the sensitivity of the calibration to the effects discussed above we have used a radiative transfer model (SBDART, Ricchiazzi *et al.* 1998). Figure 2.1 displays the calculated flux for AIRS channels 1 through 4 over a sand surface and cloudless sky, as functions of aerosol visibility, atmospheric profile, and aerosol types. It can be seen that aerosol type and visibility has a significant effect on channels 1 and 2, specifically when the visibility is low; while the water vapor amount has a significant effect on channels 3 and 4.
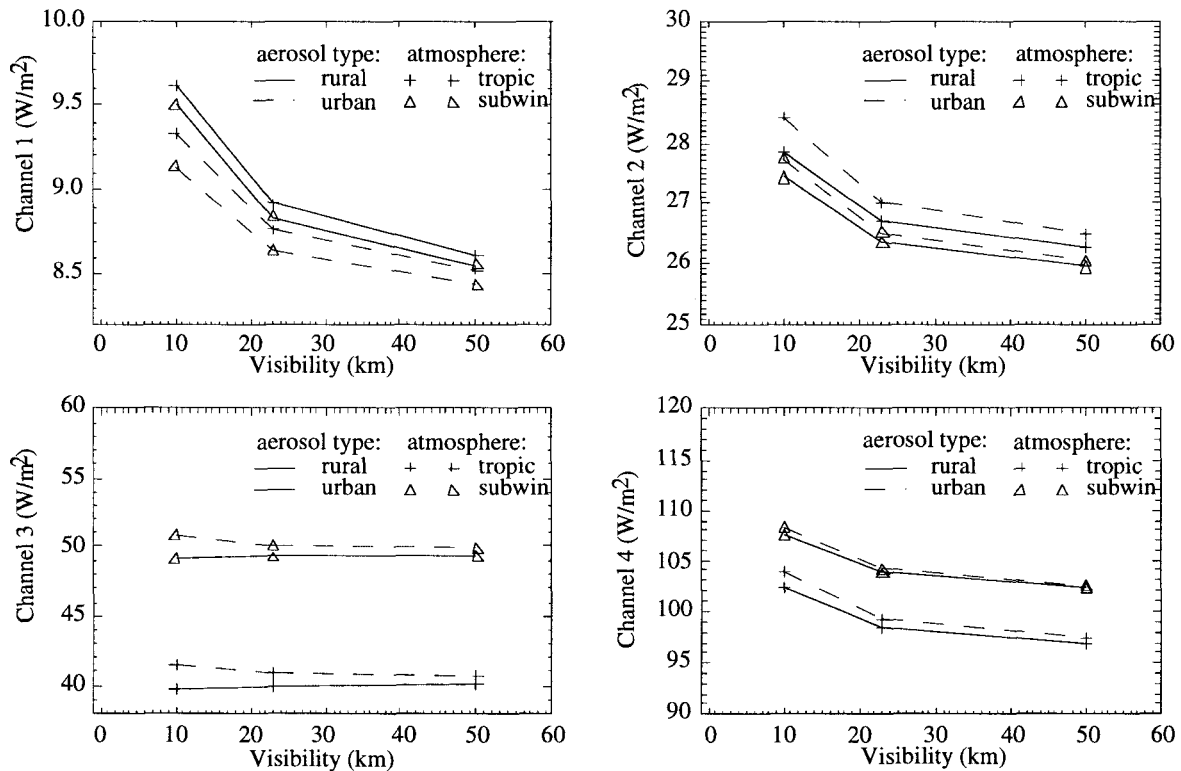
Figure 2.1: The calculated flux for AIRS channels 1 through 4 over a sand surface and cloudless sky as a function of aerosol visibility at different atmospheric profiles and aerosol types at a 30 degree solar zenith angle.

2.3.3 Data Destriping

The ground calibration target area should be homogeneous and large (e.g., White Sands, New Mexico). Though the non-linearity of detectors and electronics will have been corrected for using pre-launch information, stripes due to the array of detectors may still be present in the Vis/NIR data over homogeneous regions. A destriping procedure taking an average of 9 pixels along track would require too large an homogeneous target area. Instead, a moving window method, taking an average of 3 pixels along track, will be applied.

2.3.4 Application

Suppose the radiance calculated by the radiative transfer model is R(g) and the measured digital number is DN(g), where the subscript g is used to denote ground-based calibration. We then have:

$$\alpha(g) = \frac{R(g)}{DN(g) - DN_o}.$$ Eq. 2-5

The correction coefficient from ground-based calibration for α is then:

$$\gamma(g) = \frac{\alpha(g)}{\alpha(\text{ob})}.$$ Eq. 2-6

(No information about DN_o, the offset, can be obtained from the ground-based calibration and none is needed, since the blackbody view on every scan line is a very good zero radiance for the visible channels.)

The ground-based calibration will require clear sky atmospheric conditions. Atmospheric temperature and moisture profiles will be obtained from AIRS IR and microwave products, or from in-situ measurements made by field teams at MODIS calibration/validation ground sites. Aerosol conditions will be determined from the visibility reported by the closest meteorological station or airport (e.g. HMN, a station a few kilometers from the White Sands target area) or from MODIS field teams. Rural or continental aerosol types will be used. The surface type at White Sands is well characterized, except when wet. Precipitation events over White Sands will be monitored to determine appropriate times for calibration measurements. Surface BRDF will be either measured or modeled. A 3-D surface model is being developed for that purpose. The ground-based calibration will be carried out on a monthly basis during the operational phase.

2.4 Cross-Calibration with MODIS

2.4.1 Theoretical Basis

Step III for improving the absolute calibration is to use cross-calibration of the AIRS Vis/NIR with other instruments on the same platform, in this case with MODIS. The MODIS Spectral and Radiometric Calibration Assembly (SRCA) is traceable to a NIST standard. The SRCA will transfer the calibration to the Solar Diffuser and Solar Diffuser Stability Monitor (SD/SDSM) during the activation and evaluation phase of the instrument. The absolute radiometric uncertainty is expected to be smaller than 4.6% in-orbit (Jones *et al.* 1995). The AIRS Vis/NIR channel's cross-calibration uses a linear combination of MODIS channels. The following is a concept description. The approach will be fully developed as a research product.

Let $AIRS_i$ be the radiance from a pixel of AIRS channel i and $MODIS_j$ be the radiance from a spatially equivalent MODIS measurement from channel j. Since the AIRS FOV full width at half peak, 2250 meters at nadir, is much larger than MODIS pixels at the wavelengths in question, typically 250 to 1000 meters at nadir, AIRS spatially equivalent pixels are, in principle, obtained by convolving a gridded image of a calibration site using MODIS channel j with the AIRS spatial response function. Since the cross-calibration sites will typically be relatively homogeneous (and cloud free) desert surfaces, the requirement on spatial registration accuracy between the MODIS and AIRS pixels is relatively loose and the pre-launch determined spatial response functions will be adequate.

Figure 2.2 shows the AIRS Vis/NIR channels 1 through 4 overlaid with the spectrally similar MODIS channels. Transmittance and spectral surface albedo are plotted on the same figure. The coverage of the AIRS and MODIS channels displayed in Fig. 2.2 are listed in Table 2.1. (Note that this analysis is based on estimates of the Vis/NIR spectral response made before the flight components were available for testing. For the most up-to-date response functions, see Fig. 1.1.)

Many MODIS channels overlap, but only non-overlapping and evenly distributed MODIS channels will be linearly combined to cross-calibrate the AIRS channels. Hence, $AIRS_1$ will be cross-calibrated with $MODIS_8$ and $MODIS_9$. $AIRS_2$ will be cross-calibrated with $MODIS_1$ and $MODIS_{14}$. Because $AIRS_2$ includes water vapor absorption bands but $MODIS_1$ and $MODIS_{14}$ do not, $MODIS_{19}$ will be added to account for water vapor absorption. $AIRS_3$ will be cross-calibrated with $MODIS_2$, $MODIS_{15}$ and $MODIS_{19}$, and $AIRS_4$ with $MODIS_1$, $MODIS_2$, $MODIS_3$, $MODIS_4$, $MODIS_8$, $MODIS_{15}$, $MODIS_{19}$. This cross-calibration will be done using multivariable regressions as follows:

$$AIRS_1 = a_0 + a_1 \cdot MODIS_8 + a_2 \cdot MODIS_9 \qquad \text{Eq. 2-7}$$

$$AIRS_2 = a_0 + a_1 \cdot MODIS_1 + a_2 \cdot MODIS_{14} + a_3 \cdot MODIS_{19} \qquad \text{Eq. 2-8}$$

$$AIRS_3 = a_0 + a_1 \cdot MODIS_2 + a_2 \cdot MODIS_{15} + a_3 \cdot MODIS_{19} \qquad \text{Eq. 2-9}$$

$$AIRS_4 = a_0 + a_1 \cdot MODIS_1 + a_2 \cdot MODIS_2$$

$$+ a_3 \cdot MODIS_3 + a_4 \cdot MODIS_4$$

$$+ a_5 \cdot MODIS_8 + a_6 \cdot MODIS_{15} + a_7 \cdot MODIS_{19} \qquad \text{Eq. 2-10}$$

where, for brevity, we use the same coefficient symbols in each of the above equations, but it is understood that a_x in one equation is independent of a_x in any other equation. The coefficients a_0, a_1, ..., will be obtained using multivariate linear regression of the measured AIRS and MODIS digital numbers or radiance data. Examples are given later in this section.
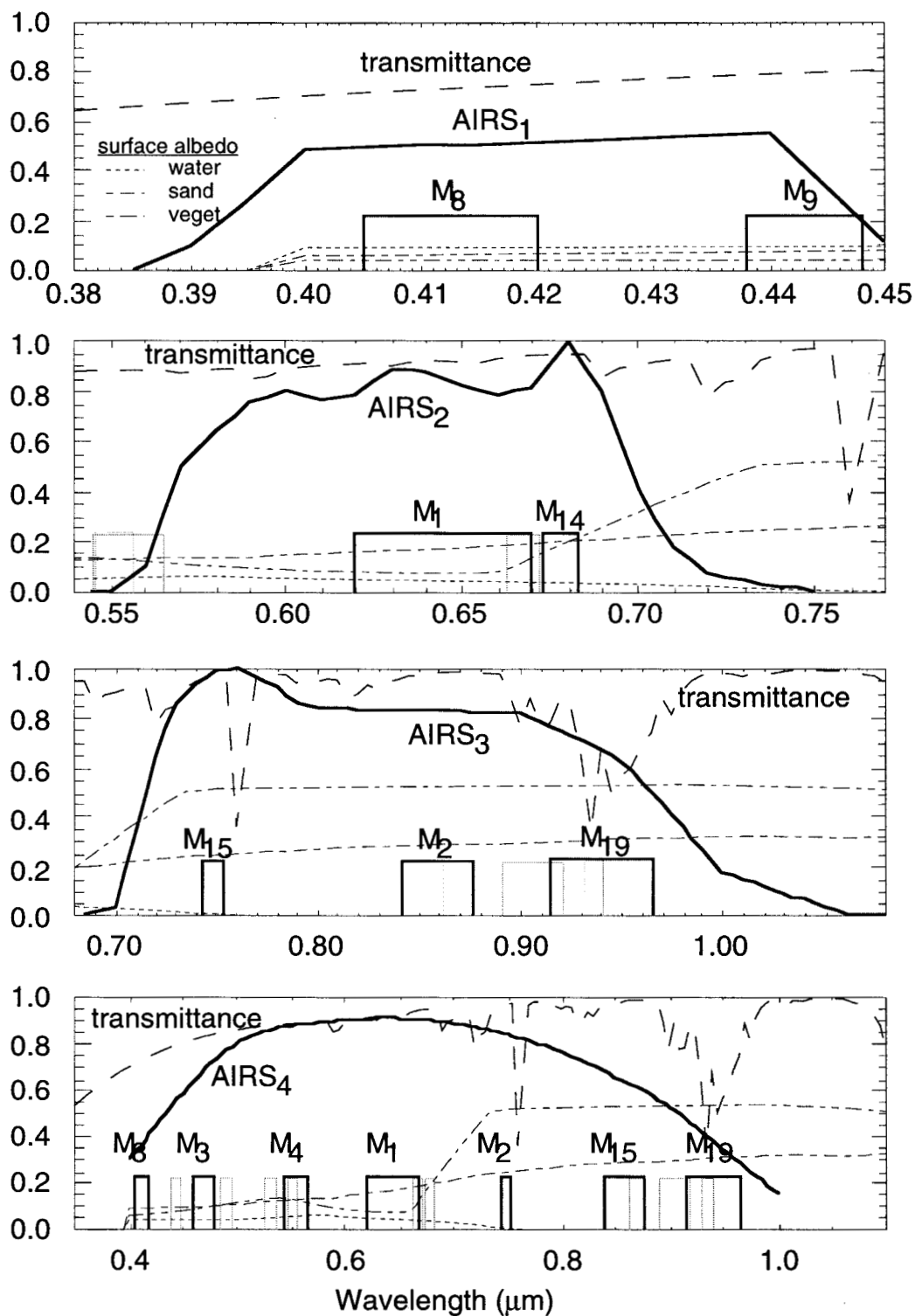
Figure 2.2: AIRS Vis/NIR channels 1 through 4 overlaid with the spectrally similar MODIS channels. Transmittance and spectral surface albedo are plotted on the same figure. Note that the AIRS response functions shown are based on estimates made before testing of the actual flight hardware. See Fig. 1.1 for the latest response functions.

It is necessary to determine what specific surface and atmospheric conditions will be most suitable for the AIRS and MODIS cross-calibration. We know that data acquired from desert area in clear sky are the best data for cross-calibration. However, we need to determine how the atmospheric profiles, specifically water vapor content, change of aerosol types and concentration, thin clouds (which may not be seen by AIRS Vis/NIR channels) and randomly distributed shrubs and shadows in the target region will affect the cross-calibration results. For this purpose, we calculated AIRS and related MODIS radiances using the SBDART radiative transfer model under the following conditions:

a) Surface cover: sand and vegetation.

b) Atmospheric profile: tropic, sub-arctic winter, and standard US atmosphere (from McClatchey *et al.* 1972), with water vapor column densities 4.12, 0.85 and 4.2 g/cm^2, respectively.

c) Cloud optical thickness: 0, 1 and 2.

d) Cloud layers: 0-1, 1-2, 2-3 and 3-4 km.

e) Cloud droplet size effective radius: 4, 8, and 16 μm for liquid, 106 μm (with cloud top height at 10 km) for cirrus ice clouds.

f) Aerosol type: rural, oceanic and urban.

g) Visibility: 10, 23 and 50 km.

The coefficients, a_i, of the linear equations (2-7) through (2-10) are calculated under three types of conditions: (i) sand surface in clear sky, (ii) sand surface in clear sky and slightly cloudy (optical depth less than 3) and, (iii) sand and vegetated surfaces in clear sky and slightly cloudy conditions. All combinations of atmospheric conditions (atmospheric profiles, aerosols and visibilities) were included in these calculations.

The linear combination of MODIS channels with respect to AIRS channels, and their fitted lines are plotted in Figs. 2.3 and 2.4 (W/m^2 is used in the plots). The coefficients of the linear equations, a_i, the correlation coefficients and standard deviation are listed in Table 2.2.
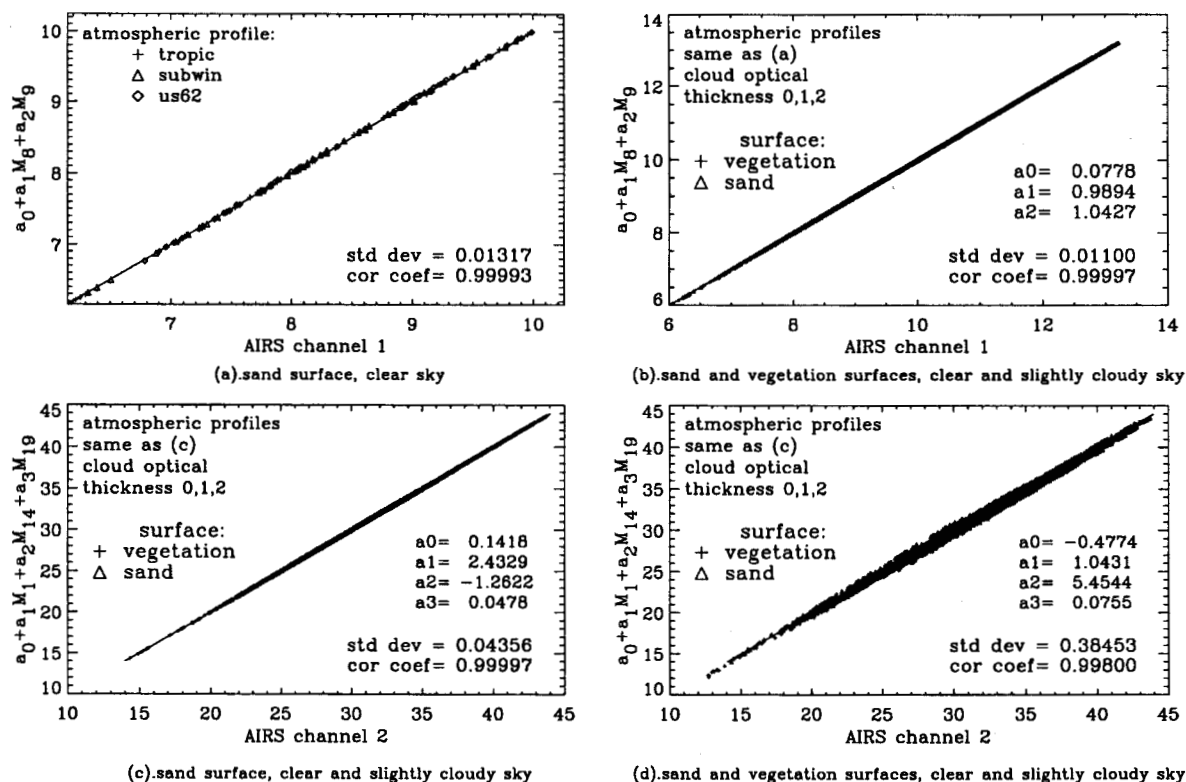
Figure 2.3: Cross-calibration of AIRS channel 1 (a and b) and 2 (c and d) using MODIS data. Panels (a) and (c) show the accuracy with which the cross-calibration can be achieved for sand surfaces. Panel (b) indicates that, even with a vegetated surface, the Ch. 1 cross-calibration is successful. For Ch. 2, however, the calibration is much poorer if vegetation is present (panel d). In these plots, calculations were made for 3 atmospheric profiles, 5 solar zenith angles, 3 aerosol types with 3 visibilities each, cloud optical thickness 0, 1 and 2 with 4 effective radii and 5 heights.

It can be seen that for $AIRS_1$ and $AIRS_4$, the coefficients calculated from sand and vegetated surfaces, in clear sky and slightly cloudy conditions (Fig. 2.3.b and Fig. 2.4.d), can fit the data as well as coefficients calculated from sand surfaces in clear sky (Fig. 2.3.a and 2.4.c). On the other hand, for channels 2 and 3, the correlation in the presence of vegetation (Fig. 2.3.d and 2.4.b) is much poorer than in the pure sand case (Fig. 2.3.c and 2.4.a).
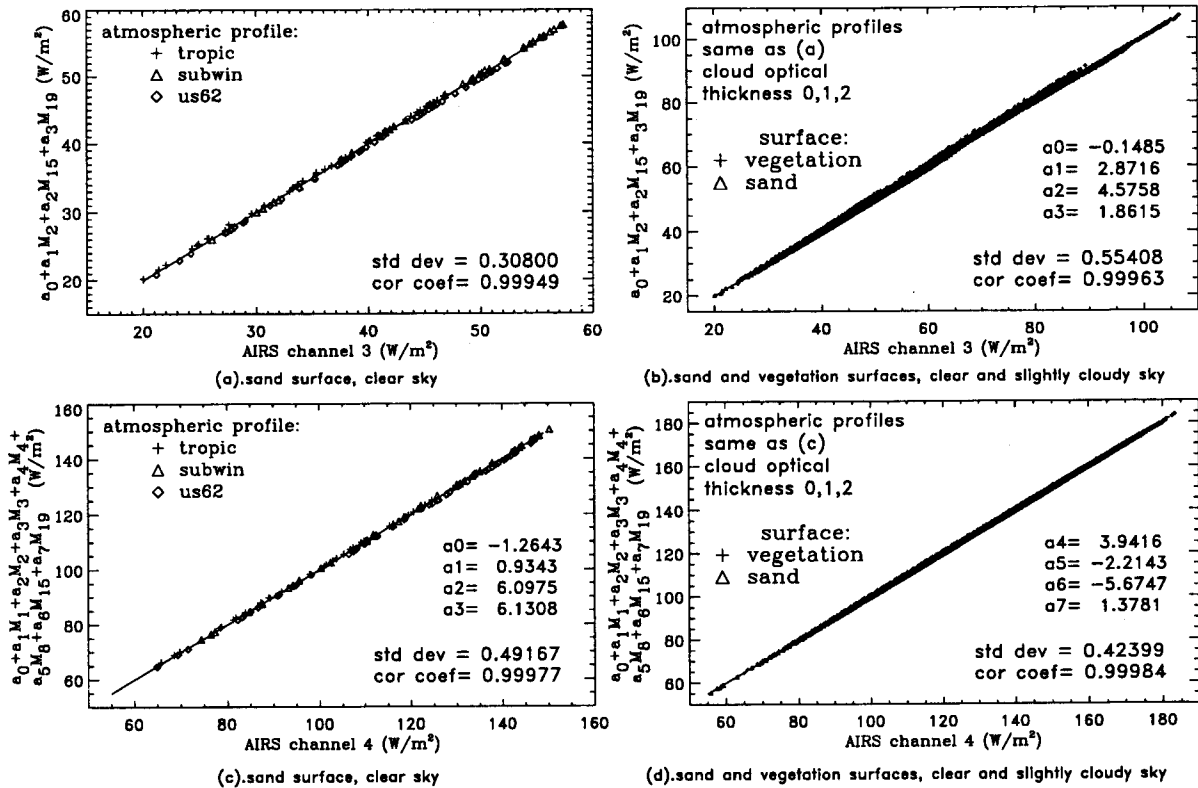
Figure 2.4: Cross-calibration of AIRS channel 3 (a and b) and 4 (c and d) using MODIS data. As in Fig. 2.3, calculations were made with 3 Atmospheric profiles, 5 solar zenith angles, 3 aerosol types with 3 visibilities each, cloud optical thickness 0, 1 and 2 with 4 effective radii at 5 heights.

This implies that only a pure desert area, like White Sands, New Mexico, can be used as a ground target for $AIRS_2$ and $AIRS_3$ cross-calibration. However, desert and semi-desert areas can be used as ground targets for $AIRS_1$ and $AIRS_4$ cross-calibration. The acceptable ground targets for the cross-calibration of $AIRS_1$ and $AIRS_4$ are therefore more abundant. It can also be seen that only the surface albedo has a significant effect on the accuracy of the cross-calibration. The influence of the atmospheric profile, aerosol type, visibility, and layer of thin clouds on the cross-calibration is negligible. This means that, unlike the ground-based calibration, no local meteorological or surface condition data are required for the cross-calibration. Therefore, the cross-calibration can be performed as frequently as required.

After 5 years in orbit, the spectral response of $AIRS_4$ is expected to degrade as shown in Fig. 1.2. Figure 2.5 shows the $AIRS_4$ radiance as a function of linear combinations of MODIS radiance data, similar to Fig 2.4, but for expected beginning and end of life conditions. Note that as the $AIRS_4$ response changes, the signal from a given ground target will change and the MODIS cross-calibration coefficients in Table 2.2 will change as well. If desired, the end-of-life $AIRS_4$ data can be restored to beginning-of-life equivalent values by assuming the linear relation

$$AIRS_{4EQ} = b_0 + b_1 \cdot x, \qquad \text{Eq. 2-11}$$

where

$$x = a_0 + a_1 \, MODIS_1 + a_2 \, MODIS_2 + a_3 \, MODIS_3$$

$$+ a_4 \, MODIS_4 + a_5 \, MODIS_8 + a_6 \, MODIS_{15}$$

$$+ a_7 \, MODIS_{19}, \qquad \text{Eq. 2-12}$$

and b_0 and b_1 will be determined from modeling or observations made in-flight over ground calibration sites. Tracking of spectral response changes is discussed further in Section 3.

Table 2.1. AIRS and Related MODIS Channels

AIRS channel	Wavelength Range (μm)	MODIS Channel	Wavelength Range (μm)
1	0.400-0.440	8	0.405-0.420
		9	0.438-0.448
2	0.550-0.745	1	0.620-0.670
		14	0.673-0.683
		19	0.915-0.965
3	0.690-1.100	15	0.743-0.753
		2	0.841-0.876
		19	0.915-0.965
4	0.400-1.000	8	0.405-0.420
		3	0.459-0.479
		4	0.545-0.565
		1	0.620-0.670
		15	0.743-0.753
		19	0.915-0.965

Table 2.2. Coefficients used in Eqs. 2-7 through 2-10: maximum difference between AIRS data and the fitted lines (in percentage): and the standard deviation. a. - sand surface as ground target b.- sand and vegetation as ground target.

	Channel 1	Channel 2	Channel 3	Channel 4
a_0	0.0778	0.1418	-0.1485	-1.2643
a_1	0.9894	2.4329	2.8716	0.9343
a_2	1.0427	-1.2622	4.5758	6.0975
a_3		0.0478	1.8615	6.1308
a_4				3.9416
a_5				-2.2143
a_6				-5.6747
a_7				1.3781
Maximum Difference (%)	0.366 [b]	0.577 [a]	2.26 [a]	1.18 [b]
Standard Dev.	0.011 [b]	0.0223 [a]	0.308 [a]	0.424 [b]

(a).sand surface, clear sky   (b).sand and vegetation surfaces, clear and slightly cloudy sky
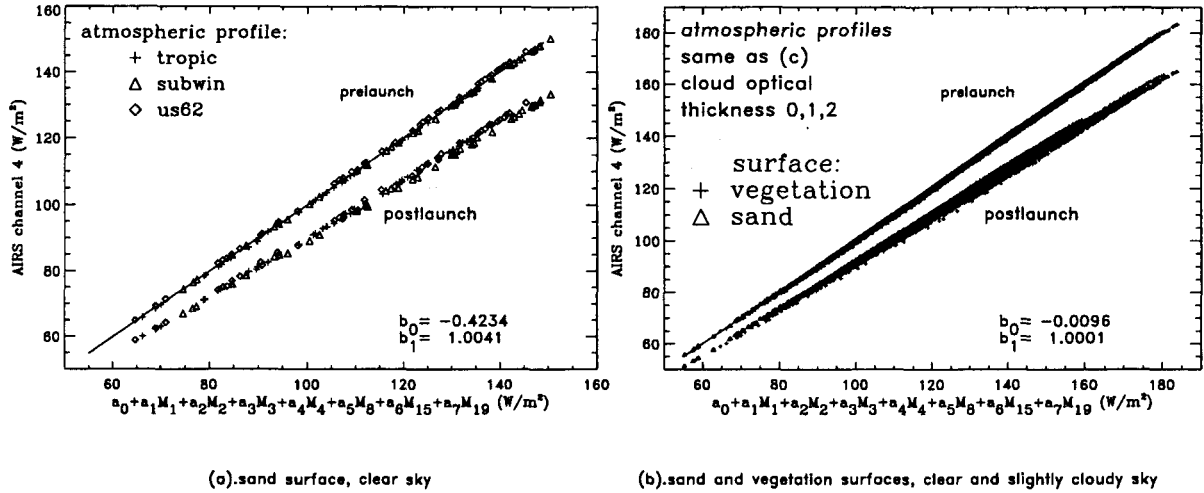
Figure 2.5: Cross-calibration of AIRS channel 4 using MODIS data. This is similar to Figs. 2.4 (c) and (d), but coefficients are calculated for both the beginning-of-life spectral response (upper curves) and the estimated spectral response of channel 4 after 5 years in-orbit (post-launch, lower).

The coefficients, a_i, in Table 2.2 are calculated based on a radiative transfer model. For practical applications, they should be calculated using real AIRS Vis/NIR and corresponding MODIS radiance data over the same ground targets to perform this cross-calibration. Therefore, it is important to spatially register the AIRS Vis/NIR channels with MODIS channels (see Section 4.3). Since a homogeneous desert surface is the best calibration area, the requirements for registration accuracy between the two are relatively loose for calibration purposes.

2.4.2 Application

The cross-calibration establishes the relationship between counts and radiance for Vis/NIR channels. After launch, in the evaluation phase, the relationship between counts of AIRS Vis/NIR channels and the linear combination of corresponding counts of MODIS channels over the target areas, given by

$$DN(e) - DN_o = a_0 + a_1 * DNM(i_1) + a_2 * DNM(i_2) + ... ,$$ Eq. 2-13

will be established as soon as possible. DN(e) and DNM are the AIRS and corresponding MODIS counts in the target areas during the cross-calibration evaluation phase. The coefficients a_0, a_1, a_2 etc. will be used later on for cross-calibration. Once MODIS radiance data is validated, the above equation will be formulated in terms of radiance as well.

After the evaluation phase, AIRS measured digital numbers over target areas, DN(ob), will be used to calculate the coefficient $\gamma(M)$:

$$\gamma(M) = \frac{DN(e) - DN_o(e)}{DN(ob) - DN_o(ob)},$$

Eq. 2-14

where $DN_o(e)$ and $DN_o(ob)$ are the dark currents (offset) measured at the time of the corresponding observations of DN. Once MODIS radiances are available, the calculation of $\gamma(M)$ will also be done in radiance-space, and a decision will be made as to which approach provides a more reliable determination. The coefficient $\gamma(M)$ will then be used to correct for any degradation of AIRS Vis/NIR channels not accounted for by on-board or vicarious calibration (if applied). Similar to the ground-based calibration, no information about DN_o is provided by the cross-calibration, but no improvements to the on-board system are needed.

Only general ground target and atmospheric condition information will be required for cross-calibration, so it will be carried out on a daily basis during the evaluation phase and on a weekly basis during the operational phase.

2.4.3 Calibration Expression

The calibration expression, Eq. 2-2, becomes

$$R = \alpha * (DN - DN_o) = \alpha(ob) * \gamma(g) * \gamma(M) * [DN - DN_o(ob)].$$

Eq. 2-15

The correction coefficients $\alpha(ob)$, $\gamma(g)$ and $\gamma(M)$ may change with time. A plot of these coefficients with respect to time will be used to study the degree and trend of any instrument degradation.

2.5 Radiometric Calibration Software

What follows is a description of the steps which will be taken to perform the visible and near-infrared radiometric calibration of the AIRS instrument. It is assumed that, during on-orbit checkout, the calibration lamps have been fully characterized via vicarious calibration over MODIS ground sites, as described in the AIRS Validation Plan (Fetzer *et al.* 1999). With minor modifications, the algorithm used for the visible is the same as the one used in the infrared channels, described in Part 1 of the Level 1b ATBD, Section 3.

2.5.1 Dataflow Description

Figure 2.6 shows a top-level diagram of the AIRS Vis/NIR radiometric calibration dataflow, from level-1A engineering units (and ancillary data) through level-1b calibrated radiances. The steps can be summarized as follows:

a) Use internal blackbody views (the infrared calibration source) to determine detector offsets.

b) Use photometric calibration target views (corrected for aging as described in 2.2.2 and 2.5.4) and calculated detector offsets to determine detector gains.

c) Apply multiplicative factors (based on observations of ground reference sites) to produce corrected detector gains.

d) Use visible and near-IR scene data numbers and calculated detector offsets and gains to produce calibrated scene radiances.
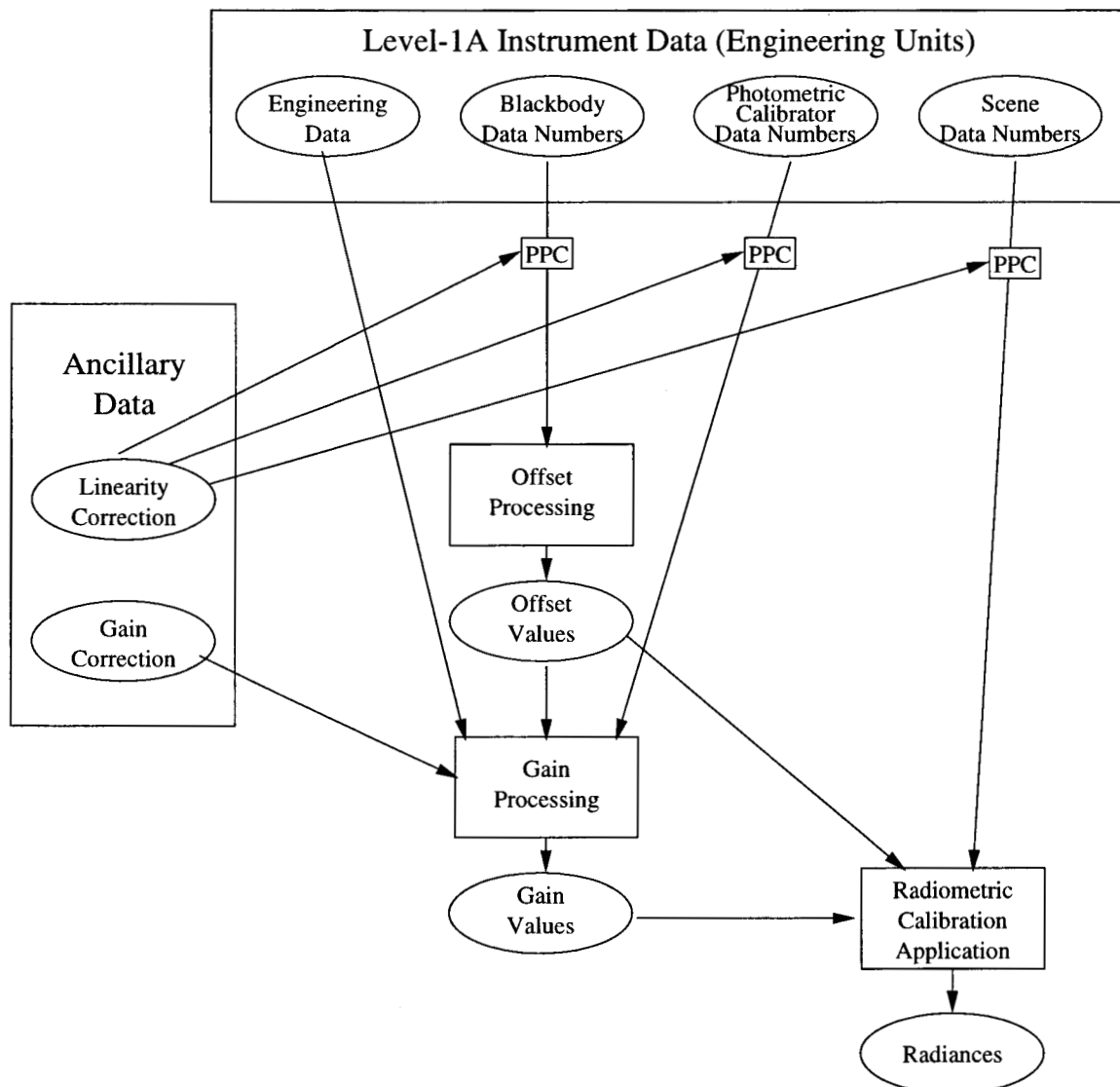
Figure 2.6: Data processing flow for Vis/NIR data. "PPC" refers to the Pre-Processing Correction described in 2.5.2.

2.5.2 Preliminary Processing Correction

Eventually, it may be desirable to perform some processing steps on each and every data number (including scene views, blackbody views, and photometric calibration target views). Because these steps can be applied directly to the input data numbers (before beginning the offset and gain calculations) they can be grouped together here as pre-processing corrections. At this time, there are no such corrections to be carried out. This section serves as a placeholder should they become necessary (such as if on-orbit checkout determines that a linearity correction is needed).

2.5.3 Offset (Dark Current) Processing

Pre-processed blackbody views are used, for each Vis/NIR channel, to determine the response of each detector pixel to a zero-radiance scene (the 310 degree Kelvin blackbody produces no significant radiance in the Vis/NIR bands). This response is in units of counts (DN).

2.5.3.1 Offset Blackbody View Selection

There are currently no selection criteria for blackbody views for Vis/NIR offset processing. That is, it is expected that all 8 views per scanline of the internal blackbody (from each pixel) will be suitable for use as Vis/NIR offset calibration footprints.

2.5.3.2 Offset Fitting (Sliding Window Approach)

Since there is noise on the blackbody views, it is desirable to combine many dark views, thereby obtaining a $\sqrt{N}$ decrease in noise levels. Because the offset level in each detector may change with time, it is desirable to fit to the smoothed variation in observed dark view counts, rather than simply taking an average.

Because we can assume that the true offset (and gain) of a detector at a given instant is reflected by measurements made close to that time, and because offset is subject to variation, it is clear that the best determination of instantaneous offset is made when the set of blackbody views which are being fit are centered on the time of interest (assuming no data drop-outs). By making this fitting "window" large (about five minutes), not only is the noise reduced, but a smoothing operation is also performed. Specifically, this approach can be expected to reduce the point-to-point variability of calculated offsets by as much as a factor of 10 (there being some 120 scan sets in five minutes). This windowing approach will work only to the extent that temperature variations of the Silicon detectors (which is the dominant factor controlling offset variations) vary smoothly within the window. This is expected to be the case and will be verified during on-orbit checkout. If offset changes are not smoothly varying the fitting window can be reduced, if necessary to the point that only a single scan line is included.

2.5.4 Gain Processing

Pre-processed views of the internal photometric calibration target are combined with calculated offset values to determine each detector's gain.

2.5.4.1 Photometric Target Radiance Calculation

The output of each photometric calibration target in absolute units (W/m^2), R_c, is determined by the pre-launch value, R_c', and correction factors. A correction is applied for aging of the bulbs based on comparisons among them (see below and Section 2.2.2) and perhaps using vicarious calibrations, as described in 2.3. The correction factor based on bulb comparisons is calculated as follows.

One bulb, designated as bulb #1 for discussion purposes, will be observed every other orbit. Bulb #2 is observed every 200 orbits, and bulb #3 is observed every 500 orbits. For any single pixel of the Vis/NIR system, let SG_i be the smoothed gain calculated when viewing bulb i, assuming the bulb output to be R_c' (the measured pre-launch value). (Gain smoothing is described in Section 2.5.4.3.) Let $K_{i,j}$ represent the ratio of smoothed gains from bulbs i and j:

$$K_{i,j} = \frac{SG_i}{SG_j}.$$

Eq. 2-16

The age corrected in-band radiance of calibration bulb 1, R_c, is then given by

$$R_c = R_c' \times K_{2,1} \times K_{3,2}.$$

Eq. 2-17

Note that each Vis/NIR pixel has its own K factors, since each pixel has a unique viewing angle to each bulb. At launch, all $K_{i,j}$ values are set to 1.0. If one bulb fails, $K_{3,2}$ is always 1.0. If two bulbs are no longer usable, both $K_{3,2}$ and $K_{2,1}$ remain identically 1.0, and vicarious calibration must be used to track bulb aging. If bulb #1 degrades in performance to the point that $K_{2,1} \leq 0.7$ (the limiting value is subject to revision based on pre-launch and on-orbit tests), it will be considered to have failed and the other operable bulbs "promoted" to more frequent use.

2.5.4.2 Instantaneous Gain Calculation

If the detector electronics measures count DN_c when viewing the internal photometric calibration target with radiance R_c, and measures count DN_o when viewing the blackbody, the instantaneous detector gain is given by

$$G = \frac{R_c}{DN_c - DN_o},$$

Eq. 2-18

in W/m²/count.

2.5.4.3 Gain Smoothing

Because there is noise on the gain calibration views, it is desirable to combine (N) gain views, thereby obtaining a $\sqrt{N}$ decrease in the noise level. Because the gain of each detector is not expected to vary significantly during the eight minutes when the photometric calibration lamp is on, it is acceptable to simply average the observed gain counts for a single eight-minute calibration cycle. This produces (for each spectral channel and for each detector pixel) a single value of gain which is representative of the eight-minute period. (Information on the stability of the gain within the eight-minute period is maintained for QA and error purposes, as described in Section 5.)

Based on experience with other visible detectors, the gain is not expected to vary appreciably even on a scale of hours. This will be verified during on-orbit checkout. Therefore, photometric calibrator target views can be averaged over several eight-minute windows, even though they are separated by many orbits. A sliding window will be used to average these infrequent gain views to the time of any observations. (Data numbers, not calculated gains, will be averaged.) Ground test data (Hofstadter 1999b) indicates that only one eight-minute period should be used for the gain of Channels 2 through 4 (achieving signal-to-noise ratios well in excess of 1000), but that two eight-minute periods should be combined for Channel 1 to insure an SNR near 100 when using calibration Lamp 3.

2.5.4.4 Vicarious Gain Correction

Because of the large uncertainty in the absolute value of the calculated gain values (due to the 20% uncertainly in absolute radiance of the photometric targets), it is desirable to correct these gain values relying on ground truth (see Section 2.3). For purposes of the operational calibration algorithm, this correction consists simply of multiplying the calculated smoothed gain values by factors, $\gamma(g)$ and $\gamma(M)$, as shown in Eq. 2-15. These correction factors are provided by the science team, and are a non-routine (research) product. The default value for the vicarious gain correction factors is 1.0 for all channels.

2.5.5 Radiometric Calibration Application

2.5.5.1 Two Point Calibration

Given the calculated offsets and gains, calibrated radiances (in units of W/m²) are obtained directly by subtracting the calculated offsets from the pre-processed observed scene counts, and multiplying this difference by the calculated instrument gain (Eq. 2-2).

2.5.5.2 Polarization and Angle-dependent Scan Mirror Correction

No explicit scan angle-dependent corrections are necessary to the Vis/NIR radiances. (The polarization effect of the scan mirror, which can be important in the infrared, is negligible for the visible channels.)

3. Spectral Calibration

The spectral response of $AIRS_1$ through $AIRS_3$ is controlled by interference filters and the spectral characteristics of the Si photodiode. The longwave region of the $AIRS_4$ channel is controlled by the spectral characteristics of the Si photodiode only. There is no on-board spectral calibration capability in the AIRS Vis/NIR instrument. However, the spectral response of the Si detectors usually shifts slowly to shorter wavelength as a function of total radiation dose (Fig. 1.2). The spectral response of the interference filters may change with time as well. Detection of change in AIRS Vis/NIR spectral response may be required. Such changes are indirectly accounted for by the calculations of $\gamma(g)$ and $\gamma(M)$ of Eq. 2-15. Because of the low spatial resolution of AIRS Vis/NIR channels (2.2 km), however, there is no homogeneous ground object which has spectral reflectivity sharp enough for good spectral calibration. This section describes a research topic (not a part of the standard AIRS processing) which may help monitor changes in the Vis/NIR spectral response.

The degradation of the spectral response of the Si photodiode will only be roughly estimated. Two approaches will be used. For $AIRS_2$ and $AIRS_3$, we will use the Amazon forest as a ground reference and the vegetation index as the parameter to monitor. The Vegetation Index is defined as:

$$VI = \frac{AIRS_3 - AIRS_2}{AIRS_3 + AIRS_2}.$$ Eq. 3-1

We will monitor the maximum value of the Vegetation Index of the Amazon forest measured by $AIRS_2$ and $AIRS_3$ to detect changes in the spectral characteristics of the system.

For evaluating the change of $AIRS_4$ spectral response, $MODIS_{15}$ (0.743-0.753) radiance can be used over any vegetated surface in clear sky conditions. Using the pre-launch spectral response of $AIRS_4$, the relationship between $AIRS_4$ and $MODIS_{15}$ is

$$AIRS_4 = 21.335 + 19.135 \, MODIS_{15}.$$ Eq. 3-2

Due to the change of $AIRS_4$ spectral response after 5 years in operation, it is expected to change to:

$$AIRS_4 = 20.976 + 16.723 \, MODIS_{15}.$$ Eq. 3-3

The correlation coefficient between these two channels is as high as 0.974. $MODIS_{15}$ is in the atmospheric window and in the longwave side of the $AIRS_4$ channel, hence it is least affected by water vapor content and aerosol type and concentration (Fig. 3.1a). As a comparison, the correlation coefficient of $AIRS_4$ to other MODIS channels is much smaller as shown by the plot of $AIRS_4$ with respect to $MODIS_3$ (Fig. 3.1b).

(a). AIRS channel 4 with respect to MODIS channel 15   (b). AIRS channel 4 with respect to MODIS channel 3
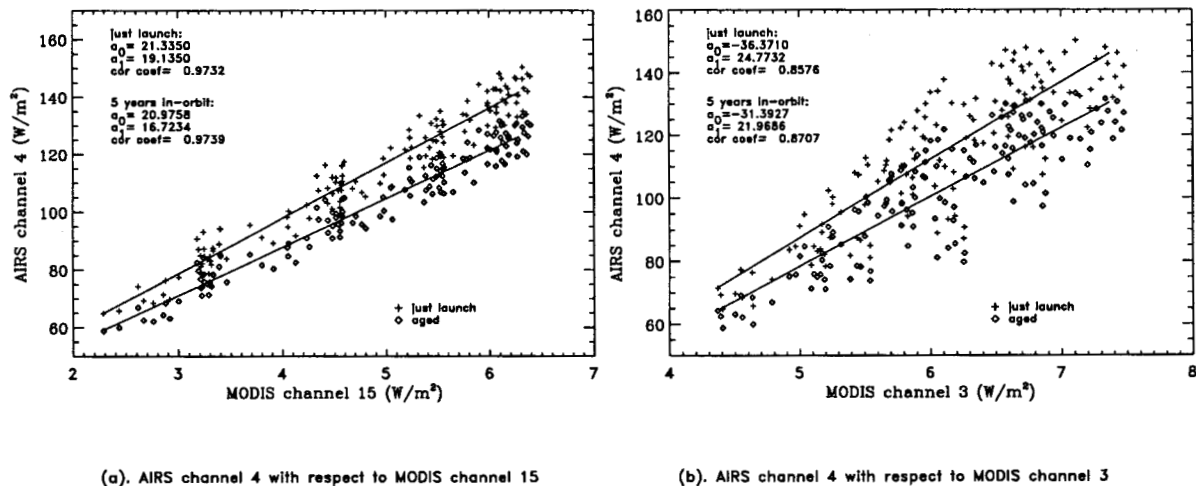
Figure 3.1: The change of spectral response of AIRS channel 4 can be detected by the ratio of AIRS channel 4 to MODIS channel 15 (left) over a vegetated surface in clear sky conditions. The atmospheric profile and aerosols have a stronger effect on MODIS Channel 3.

4. Spatial Calibration

4.1 Geolocation and Co-Alignment of Vis/NIR Channels

Previous versions of this document presented a discussion of how observations of coastline crossings could be used on-orbit to improve our knowledge of the spatial calibration (the pointing) of the Vis/NIR detectors. A more advanced algorithm has since been developed, and is maintained as a separate document, Jovanovic and Hofstadter (1997). Only a brief summary is presented here.

The first step in geolocation is to assemble a detailed instrument geometric model. This is a mathematical relation describing the line-of-sight vector associated with any pixel in terms of the instrument coordinate system. A transformation from instrument to spacecraft coordinate systems is also included. Table 4.1 lists the basic parameters and their nominal values. An additional component of the instrument model is a covariance matrix describing how each model parameter depends on all other parameters, and how a pixel's longitude and latitude depends on each parameter.

Most of the parameters in Table 4.1 are self-explanatory. To allow for non-linearities in the instrument scan rate across-track, a polynomial can be determined relating across track column number to the column number that would result from a perfectly uniform scan. (Non-linearities can arise in either the scan mirror motion or the detector readout process.) The array indicated holds coefficients for a third order polynomial: shown is the nominal case of uniform sampling. The "Time offset between channels" parameter allows for a systematic time delay between readouts of each Vis/NIR channel: its nominal value is zero because all channels are supposed to be sampled simultaneously. Each of the parameters in Table 4.1 has been measured on the ground, and a subset will be verified/refined using in-flight calibration.

Table 4.1. Vis/NIR Instrument Geometric Model

Geometric Parameters	Nominal Value
Effective Focal Length	77.427 mm
Number of pixels across-track in one scan line	720
Number of pixels along-track in one scan line	9
Coefficients to account for non-linearity of scan rate	[0, 1, 0, 0]
Scan mirror tilt	45°
Total across-track angular coverage in one scan line	99.0°
Total along-track angular coverage in one scan line	1.665°
Misalignment between instrument coordinate system and spacecraft coordinate system [roll, pitch, yaw]	[0°, 0°, 0°]
Scan mirror rotation period	2.667 sec
Interval between reading consecutive pixels in an array	6.0E-5 sec
Interval between consecutive readouts of the same pixel	2.801E-3 sec
Time offset between channels	0 sec

The instrument model, combined with absolute time information, spacecraft ephemeris data, and an Earth model, allows any pixel in an image to be assigned to an Earth longitude and latitude. The second step in spatial calibration is to assemble a data base of Ground Control Points (GCP's), which are easily located features for which extremely accurate geocentric positions are known. (Small islands make excellent GCP's, and they can be recognized both by the two-dimensional shape of their land/ocean interface and by the albedo statistics associated with a given radius from their center. These two recognition schemes are called feature-based and area-based matching, respectively.) By locating the GCP's in flight data, and comparing their calculated geocentric positions with their known locations, the instrument pointing can be validated or updated. An update is performed by using a least-

squares regression to modify the instrument model in such a way as to minimize the difference between calculated and known positions in a large sampling of GCP's.

The spatial calibration technique just described can be used to update the relative pointing of the four Vis/NIR channels as well as their absolute Earth coordinates. With this approach, geolocation to within 10% of a pixel (~200 m at nadir) is straightforward, and location to 1% of a pixel (~20 m at nadir) should be possible.

4.2 Spatial Calibration of Visible Channels to the Infrared

Excluding research products, the primary purpose of the visible channels is to provide statistical information on cloud structures and surface inhomogeneities within an infrared footprint. For these purposes, it is sufficient that the visible and IR instruments be aligned to within half of a visible pixel. The previous section pointed out that it is straightforward to locate the visible channels with respect to the spacecraft boresight to within 0.1 visible pixels (about 200 meters on the ground at nadir). Section 5.1 of Part 1 of the Level 1b ATBD found the IR footprint can be determined to ~1% of the IR field of view, which is 0.06 Vis/NIR pixels. The combined uncertainty between the IR and Vis/NIR boresights is then ~0.12 Vis/NIR pixels, well within the 0.5 pixel requirement.

4.3 Co-Alignment of the MODIS and AIRS Instruments

The MODIS instrument observes in the visible and infrared, with nadir spatial resolution of about 0.2 km at visible wavelengths, and 1 km in the infrared. (This compares to the 2.3 km size, at nadir, of a Vis/NIR pixel.) Pre-launch calibration of MODIS allows its orientation relative to the spacecraft boresight to be known to better than 0.2 MODIS pixels. Combining this uncertainty with the 0.1 to 0.01 Vis/NIR pixel uncertainty in the AIRS boresight (discussed in 4.1) yields a pointing alignment between MODIS and AIRS visible channels of 0.10 to 0.02 Vis/NIR pixels. Similarly, the pointing between MODIS IR channels and AIRS Vis/NIR channels is accurate to 0.13 to 0.09 Vis/NIR pixels.

Some potential uses of MODIS data by AIRS are improved radiometric calibration of the AIRS visible channels (discussed in Section 2.4), and statistical studies of variability on scales smaller than an AIRS visible pixel. For these purposes, alignment of AIRS and MODIS to ~0.1 of an AIRS visible pixel is sufficient. The estimates in the previous paragraph indicate that this requirement is met (albeit marginally for the MODIS IR channels) by the pre-launch spatial calibration of MODIS. The on-orbit spatial calibration routine described in Section 4.1 will be used to correct for any alignment changes resulting from launch or gravity release, and will eventually result in a spatial calibration more accurate than that determined pre-launch.

4.4 Gridding and Mapping Considerations

While not formally a part of the Level 1b product, brief mention will be made of the following data processing tasks: mapping of visible data, combining of visible and infrared data, and quality control of mapped data.

4.4.1 Mapping of Visible Data

As the scan mirror rotates to view across track, the projection of each visible detector on the ground rotates and stretches due to geometric effects. A transform function will be derived that translates pixel element number and scan angle into geocentric coordinates. Since Vis/NIR oversamples the ground (see Section 1.3), averaging and resampling can be used to create maps from this geolocated data with a signal-to-noise ratio slightly higher than that of the raw data. (Alternatively, sub-pixel resolution is possible on sharp features.) Resampling of data also allows all Vis/NIR channels to be reported on a common grid, accounting for any possible misalignments between the channels revealed by ground or on-orbit spatial calibration. All of these mapping activities will be pursued as research products.

4.4.2 Gridding of Visible and Infrared Data

The offsets between visible and infrared data (Section 4.2) will be used to map the visible data onto the infrared's data grid. Unlike the pure visible case, however, the different footprints of the data sets must be accounted for. A beam pattern will be calculated for the infrared data, and this smoothing applied to the visible data. The smoothed visible data can then be directly compared to the infrared.

4.4.3 Mapped Data Quality Control and Quality Assessment

At this time, the only automatic Quality Control anticipated for mapped data is charged particle circumvention. Charged particles striking the visible detectors can create spurious signals. Most "upset" pixels can be recognized by their large deviations from neighboring, overlapping pixels. Whenever a pixel readout contains a value differing from the average value of its overlapping neighbors by more than a 3-sigma noise estimate, that pixel will be rejected.

The entire AIRS Quality Assessment plan is currently being refined, and is maintained as a separate document. See the EOS or AIRS homepages for the most current version (http://www-airs.jpl.nasa.gov or http://eospso.gsfc.nasa.gov).

5. Level 1 Quality Control/Error Estimates/Exception Handling

5.1 Quality Control

Quality of level-1b products is ensured primarily by the routine analysis of the level 1b and level-2 products of selected ground sites which are observed as part of the normal spatial coverage. The algorithm for this task is a team member research product. Variations and trends in the correction terms of Eqs. 2-15 and 2-17 ($\gamma(g)$, $\gamma(M)$, and $K_{i,j}$) may also be part of this algorithm.

5.2 Error Estimates

Uncertainties in the level-1b products (offsets, gains, and radiances) are quantified based on three primary indicators and one secondary indicator. The first primary indicator is the quality of the fits that are done to offset and gain. These quality indicators are in the form of correlation coefficients. The second indicator is the observed variance of the signal from the photocalibration source during the 8 minutes the bulb is on. The third primary quality indicator is the availability of calibration data. If many dark view or photocalibration footprints are missing over a time interval, we know that the noise level will be higher. Each of these concepts will be developed quantitatively using experience gained with the flight model.

A secondary indicator of data uncertainty is the magnitude of the discrepancy between the routinely produced data from a ground calibration site and the truth. The algorithm for this estimate is a research task of an AIRS team member, and is related to vicarious calibration.

5.3 Exception Handling

Because the level-1A processing will have analyzed the quality of the instrument telemetry (testing for completeness and corruption), no garbled data should be processed. The only exception currently anticipated is the possibility of data drop-outs (gaps), and the impact of these on level-1b processing is minimal. If scene footprints are missing, they are simply not calibrated. If offset (blackbody) calibration footprints are missing, there should be plenty of others within an averaging window with which to work. If gain (photometric calibrator) calibration footprints are missing, the most recent good data will be used instead, and the quality indicators will be modified accordingly. Other exceptions (notably spurious data) can be handled in the Level 2 product generation routines (such as mapping, see Section 4.4.3).

6. Appendix A: List of Acronyms

ADC	Analog to Digital converter
AIRS	Atmospheric Infrared Sounder
ACT	Across-Track
ALT	Along-Track
AMSU	Advanced Microwave Sounding Unit
ATBD	Algorithm Theoretical Basis Document
ATCF	AIRS Test and Calibration Facility (TVAC)
AVHRR	Advanced Very High Resolution Radiometer
BRDF	Bi-directional Reflectance Distribution Function
CSV	Cold Space View
DCR	DC Restore (of the electronics)
DN	Data Number
DOD	Department of Defense
EM	Engineering Model
EOS	Earth Observing System
FOV	Field of View (projected on the ground pertaining to one dwell time)
FM	Flight Model
FRD	Functional Requirements Document
FWHM	Full Width at Half Maximum
GCP	Ground Control Point
GSFC	Goddard Space Flight Center
HgCdTe	Mercury-Cadmium Telluride
HIRS	High Resolution Infrared Sounder
HSB	Humidity Sounder Brazil
IFOV	Instantaneous Field of View. Smaller or equal to the FOV.
IR	Infrared
ITS	Interagency Temperature Sounder
JPL	Jet Propulsion Laboratory
LMIRIS	Lockheed-Martin Infrared Imaging Systems
MODIS	Moderate Resolution Imaging System (on EOS-AM and PM)
MSU	Microwave Sounding Unit
NASA	National Aeronautics and Space Administration
NEDT	Noise Equivalent Delta Temperature
NEN	Noise Equivalent Radiance
NIR	Near Infrared
NIST	National Institute of Standards
NOAA	National Oceanic and Atmospheric Administration
NWS	National Weather Service
OBC	On-Board Blackbody Calibrator
OBS	On-Board Spectral reference source
PC	Photoconductive Detector
PFM	Proto Flight Model
PPC	Pre-Processing Correction
PRT	Platinum Resistance Thermometer
PV	Photo Voltaic Detector
QA	Quality Assessment
SBDART	Santa Barbara Discrete-ordinate Atmospheric Radiative Transfer
SNR	Signal to Noise Ratio
SRF	Spectral Response Function
TBD	To Be Determined

TVAC   Thermal Vacuum Chamber
VIS   Visible wavelength

7. Appendix B: Response to Reviewer's Comments

Version 1.1 of this document underwent EOS Project review in March 1997. Comments were conveyed to the AIRS Project in July 1997. Relevant comments are summarized below.

Comments from write-in reviewer Robert Benjamin Lee III:

1) Why isn't cold space used as a zero-radiance target?

RESPONSE: The blackbody is expected to provide a more uniform target, with less chance of Earth or Moon light contaminating the signal.

2) Because the photodiode's response varies with temperature, the zero-radiance offset may be different observing a 308 K blackbody than observing the 255 K typical longwave radiances of the Earth. Will corrections account for this?

RESPONSE: A correction is not necessary because scene temperature does not dominate the detector temperature and the detector thermal inertia prevents large changes over the 2.7 second scan period. None-the-less, the temperature of the detectors is monitored within each scan and a correction can be applied should it become necessary.

3) The photodiode response can change with time due to water contamination. What long-term changes are expected and what corrections will be applied?

RESPONSE: Sections 2.3, 2.4 and 3.0 discuss vicarious calibration, cross calibration, and spectral calibration algorithms. These approaches are used to correct for aging of all components of the system.

4) Cross-calibration with MODIS should be described in more detail, especially how the smaller MODIS spatial response functions will be compared to the larger AIRS footprints.

RESPONSE: Cross-calibration is a research product to be refined after launch, and information on the AIRS and MODIS spatial response functions are not yet available. Details are therefore not available.

Comment from panel reviewer Paul Menzel:

5) High spatial resolution data from AIRS Vis/NIR and from MODIS could improve the AIRS cloud-clearing algorithm. Consider this approach, and encourage further collaboration between AIRS and MODIS.

RESPONSE: One of the primary purposes of the AIRS Vis/NIR channels is to provide information on cloud amount (Section 1.2). Initially this information is used for QA purposes, but as a Research Product Vis/NIR data will be incorporated into the AIRS retrieval (see the Level 2 ATBD). To improve communication with the MODIS Team, AIRS has a designated representative to attend MODIS Science Team meetings and develop familiarity with MODIS retrieval, calibration, and validation activities. Several meetings

between AIRS team members and MODIS calibration team members have also been used to coordinate validation and calibration activities.

8. Appendix C: Change Summaries

Changes, Version 1.1 to Version 2.0

This section summarizes the substantive changes made in Part 2 of the AIRS Level 1b ATBD (dealing with the Visible/Near-Infrared Channels), in going from Version 1.1 (the first release, dated 15 November 1996) to Version 2.0 (dated 4 January 1999). Unless explicitly stated, all page and section references apply to the new version of the document.

The most obvious change is a complete restructuring. The old ATBD combined the IR and Vis/NIR detectors into a single document, while the new version has separate documents for each. In addition, the new version brings related discussions together that previously were separate (for example, software descriptions now appear in the same sections as the corresponding algorithms). The document has also been stylistically edited to make sections written by different authors more consistent and understandable.

The Vis/NIR instrument overview (Section 1.3) has been updated to reflect "as built" properties, including measurements of the flight-hardware spectral response, the removal of the precision-reference-diodes from the calibration system, and the oversampling of the across-track direction.

Changes in the Radiometric Calibration discussion (Section 2) include:
- Variable names have been made consistent between the algorithm and software discussions.
- The description of the photocalibration lamps has been updated to reflect the as-built voltage of the system, the estimated lifetime of the bulbs, and a new scheme for tracking bulb changes with use.
- Tables 2.1 and 2.2 (page 23) have parameters inserted that were missing from Version 1.1.
- The software discussion (Section 2.5) and flow charts have been updated to reflect the removal of the precision reference diodes and the incorporation of the "rotating" bulb scheme to track bulb aging.
- Several partially redundant sub-sections have been combined into single discussions.
- More details are provided in the discussion of offset and gain averaging/smoothing.

The Spatial Calibration discussion (Section 4) has been totally rewritten to reflect a more advanced algorithm, but defers all details to the separate Geolocation document written by Jovanovic and Hofstadter.

Minor additions were made to the discussion of Quality Control and Error Estimates (Section 5).

Finally, Appendices (Sections 6 and 7) were added to discuss reviewer comments received on Version 1.1, and to record changes to the document.

Changes, Version 2.0 to Version 2.1

The substantive changes made during the December 1999 update are:
- Account for new information on mirror spectral response (Section 1.3).
- Account for subsampling of the surface (Section 1.3).
- Account for new information on calibration lamp performance (Sections 2.2.2, 2.2.4, and 2.5.4.3).
- Update various parts of Chapters 2 and 6 to reflect recent discussions with MODIS.

- Remove the linearity correction from Section 2.5.2.
- Account for new timing information in Table 4.1.
- Add a list of acronyms (Appendix A).

9. References

Abel P. (1991). Clouds As Calibration Targets For AVHRR Reflected-solar Channels: Results From a Two-year Study At NOAA/NESDIS. *SPIE* **1493**, 195-206.

Aumann, H.H. and C. Miller (1995). Atmospheric Infrared Sounder (AIRS) on the EOS Observing System. *SPIE* **2583**, 332-343.

Brest, C. L. and W. B. Rossow (1992). Radiometric Calibration and Monitoring of NOAA AVHRR Data For ISCCP. *Int. J. Remote Sensing* **13**, 235-273.

Che, N., B. G. Grant, D. E. Flittner, P. N. Slater and S. F. Bigger (1991). Results of Calibration of the NOAA-11 AVHRR Made By Reference To Calibrated SPOT Imagery At White Sands, N. M.. *SPIE* **1493**, 182-194.

Che, N and J. C. Price (1992). Survey of Radiometric Calibration Results and Methods For Visible and Near-Infrared Channels of NOAA-7, -9 and -11 AVHRRs. *Remote Sensing of Environment* **41**, 19-27.

Fetzer, E., M. Gunson, E. Fishbein, S. Granger, D. Hagan, M. Hofstadter, B. Lambrigtsen, E. Olsen, S.Y. Lee (1999). AIRS Team Science Data Validation Plan. JPL Document D-16822, Version 2.0, Dec 1999.

Fraser, R. S. and Y. J. Kaufman, (1985). Calibration of Satellite Sensors After Launch. *Applied Optics* **25**, No. 7, April, 1986.

Frouin, R., and C. Gautier (1987). Calibration of NOAA-7, GOES-5 and GOES-6 VISSR/VAS Solar Channels. *Remote Sensing of Environment* **22**, 73-101.

Guenther, B. W., R. Gilmore, B.L. Markham, and J. Cooper (1990). Result From the NASA ER-2 Aircraft Experiment at White Sand, N.M.. *Meeting on Radiometric Calibration of Satellite Sensors of Reflected Solar Radiation* NOAA/NESDIS, March 27-28.

Hofstadter, M.D. (1998). Lifetime of Vis Calibration Lamps: Implications for the Calibration Cycle. AIRS Science Design File, document ASDF-0026-1998-MDH.

Hofstadter, M.D. (1999a). AIRS Vis/NIR Spectral Response. AIRS Design File, document ADF-346.

Hofstadter, M.D. (1999b). Review of Pre-Vibration Vis/NIR Test Data. AIRS Design File, document ADF-352.

Holben B. N., Y. J. Kaufman and J. D. Kendall (1990). NOAA-11 AVHRR Visible and Near-IR Inflight Calibration. *Int. J. Remote Sensing* **11**, 1511-1519.

Jones, M., H. Montgomery, R. Veiga, D. Knowles, N. Che and I. L. Goldberg. *MODIS Level 1b Algorithm Theoretical Basis Document 1995 [MOD-02].*GSFC, SBRC.

Jovanovic, V.M. and M.D. Hofstadter (1997). AIRS Vis/NIR Geolocation Algorithm. AIRS Design File, document ADF-265.

McClatchey, R.A., R.W. Fenn, J.E.A. Selby, F.E. Volz, and J.S. Garing (1972). *Optical Properties of the Atmosphere*, 3rd Ed. AFCGRL-72-0497, 113 pp.

Price J. C. (1987). Radiometric Calibration of Satellite Sensors in the Visible and Near-Infrared: History and Outlook. *Int. J. Remote Sensing* **22**, 3-9.

Ricchiazzi P., S. Yang and C. Gautier (1998). SBDART: A Research and Teaching Software Tool for Plane-Parallel Radiative Transfer in the Earth's Atmosphere. *Bull. Am. Met. Soc.* **79** (10), 2101-2114.

Slater, P.N., S. F. Biggar, and J. M. Palmer (1991). Ground-reference Site and On-board Method For Sensor Absolute Calibration in the 0.4 to 2.5 µm Range. *Proc. Helsinki IGARRS '91.*

Slater, P.N., S. F. Biggar, R. G. Holm, R. D. Jackson, Y. Mao, M. S. Moran, J. M. Palmer, and B. Yuan (1987). Reflectance- and Radiance-based Methods for the In-flight Absolute Calibration of Multispectral Sensors. *Remote Sensing of Environment* **22**, 11-37.

Walraven, R. L. and K.L. Coulson (1972). Measurements of Light Properties of Gypsum Sand. *Contrib. Atmos. Sci.* **7**, Univ. of California, Davis.